ChemComm

COMMUNICATION

View Article Online
View Journal

Cite this: DOI: 10.1039/c8cc07709f

Received 25th September 2018,
Accepted 28th November 2018

DOI: 10.1039/c8cc07709f

rsc.li/chemcomm

Water as a structure-driving agent between the UiO-66 and MIL-140A metal–organic frameworks†

Vera V. Butova,*[a] Andriy P. Budnyk,[a] Konstantin M. Charykov,[a] Kristina S. Vetlitsyna-Novikova,[a] Carlo Lamberti *[ab] and Alexander V. Soldatov[a]

We report a careful investigation of a selective phase formation in the zirconium–terephthalic acid system during solvothermal synthesis, which could result in the UiO-66 ($Zr_6O_6(OH)_4(BDC)_6$) or MIL-140A (ZrO(BDC)) metal–organic frameworks (MOFs). The introduction of water varies the phase from MIL-140A to UiO-66 by producing at the nucleation stage tetragonal ZrO_2 nanoparticles, where the local arrangement of Zr and O atoms is similar to that in the UiO-66 SBU.

MOFs are porous crystalline materials showing numerous applications.[1–7] According to the reticular design concept, the structure of MOFs can be conditionally divided into two components: inorganic metal clusters – secondary building units (SBUs) – and organic molecules acting as linkers.[8] Ideally, the combination of a certain metal center with a given linker molecule leads to a unique type of MOF topology. However, there are several cases reported, where starting from the same components and using different synthesis techniques one could obtain chemically similar MOFs of various structural arrangements, named as "polymorphs" or "framework isomers".[9] An example of such a phenomenon is the UiO-66/MIL-140A system. Both MOFs consist of zirconium ions and benzene-1,4-dicarboxylate (BDC) linkers (hereafter Zr-BDC MOFs), however they possess two different topologies: UiO-66 has a cubic symmetry and a 3D pore system,[10–17] and MIL-140A forms a monoclinic phase with 1D triangular channels.[18,19] As different structures result in different properties of the final material, it is mandatory to have full control on the nature of the synthesis products when moving in the multidimensional space of the synthesis parameters. The high stability of UiO-66-67-68 family[10–17] has stimulated different kinds of functionalization aimed to obtain efficient heterogeneous catalysts;[20–28] because of all this interest, the understanding of the growth conditions of UiO MOFs is particularly relevant.

In the present work, we prepared a series of samples with molar ratios of Zr^{4+} : BDC of 1 : 1 and 1 : 2 and at two synthesis temperatures (120 and 220 °C being the most used according to the literature survey reported in Table S1 of the ESI†).[11,13,18] To investigate the effect of water addition, we then split each synthetic route into cases with water and without water (see Section S2 in the ESI†). The synthesis parameters for all samples are provided in Table 1.

All syntheses performed at 120 °C yielded single phase UiO-66, independently of the other parameters (molar ratio of the components and presence of water), see Table 1 and Fig. 1a for the X-ray powder diffraction (XRPD) patterns. For the samples synthesized in the absence of water (1:1:0_120-UiO and 1:2:0_120-UiO), the only minor difference lies in a much lower relative intensity of the (022) reflection around $2\theta \approx 12^\circ$, typical of dehydroxylated distorted Zr_6O_6 octahedra as SBUs.[11,29,30] This suggests that the presence of water is needed to obtain the perfect UiO-66 structure with symmetrical $Zr_6(OH)_4O_4$ octahedra as SBUs. For the syntheses performed at 220 °C, either the UiO-66 or MIL-140A phases could be obtained depending on the synthesis conditions (Fig. 1c and Table 1). Addition of water to the reaction mixture results in the formation of the UiO-66 phase at any of the investigated Zr : BDC ratios (1 : 1 and 1 : 2), while in absence of water the only crystalline product is the MIL-140A phase, which is formed at a Zr : BDC ratio of 1 : 2, otherwise an amorphous phase dominates the synthesis (Fig. 1c and Table 1).

The FTIR spectra of samples obtained at 120 °C (Fig. 1b) agree with those previously reported for UiO-66, where the most peculiar feature is the 665 cm^{-1}-band, assigned to a vibration of the $Zr_6(OH)_4O_4$ cluster.[11,29] According to the XRPD data, the IR spectra of samples obtained at 220 °C differ from each other: samples 1:1:3_220-UiO and 1:2:3_220-UiO exhibit the modes of

[a] The Smart Materials Research Institute, Southern Federal University, Sladkova str. 178/24, Rostov-on-Don, 344090, Russia. E-mail: butovav86@gmail.com

[b] Department of Physics, INSTM Reference Center and CrisDi and NIS Interdepartmental Centers, University of Turin, Via P. Giuria 1, 10125 Turin, Italy. E-mail: carlo.lamberti@unito.it

† Electronic supplementary information (ESI) available: Survey on the different synthesis parameters reported in the literature for UiO-66 and MIL-140A; XRPD patterns in the full 2θ profile; TGA curves and N_2 adsorption isotherms; magnified FTIR spectra; TEM and XRPD study of thermally decomposed UiO-66. See DOI: 10.1039/c8cc07709f

Table 1 Synthesis parameters for Zr-BDC MOFs and phase composition of the product according to XRPD and FTIR data

		Molar ratio of components				Product	
Sample name	Synthesis temp. (°C)	DMF	$ZrCl_4$	BDC	H_2O	Long-range order (XRPD)	Short-range order (FTIR)
1:1:3_120-UiO	120	300	1	1	3	UiO-66	UiO-66
1:1:0_120-UiO	120	300	1	1	0	UiO-66	UiO-66
1:2:3_120-UiO	120	300	1	2	3	UiO-66	UiO-66
1:2:0_120-UiO	120	300	1	2	0	UiO-66	UiO-66
1:1:3_220-UiO	220	300	1	1	3	UiO-66	UiO-66
1:1:0_220-amor	220	300	1	1	0	Amorphous	MIL-140A
1:2:3_220-UiO	220	300	1	2	3	UiO-66	UiO-66
1:2:0_220-MIL	220	300	1	2	0	MIL-140A (55%) + amorphous (45%)	MIL-140A
1:2:0_220_M-ZrO_2-MIL	220	300	1	2	0	MIL-140A (30%) + amorphous (70%)	MIL-140A
1:2:0_220_T-ZrO_2-UiO	220	300	1	2	0	UiO-66	UiO-66

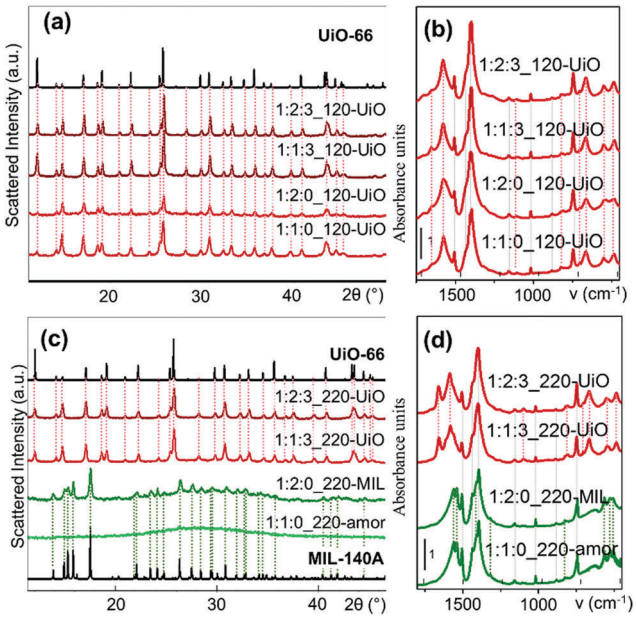

Fig. 1 Part (a): XRPD profiles (λ = 1.5406 Å) measured for samples synthesized at 120 °C (see Table 1). The patterns labelled as UiO-66 and MIL-140A are calculated from the literature cif data for UiO-66[12] and MIL-140A.[18] Part (b): FTIR spectra of desolvated samples synthesized at 120 °C. Parts (c) and (d), same as parts (a) and (b), for samples synthesized at 220 °C. Patterns and spectra have been vertically translated for clarity. The two main reflections, (111) and (002), have been excluded to enhance the visibility of the higher reflections, see Fig S1a and b in the ESI† for the full patterns.

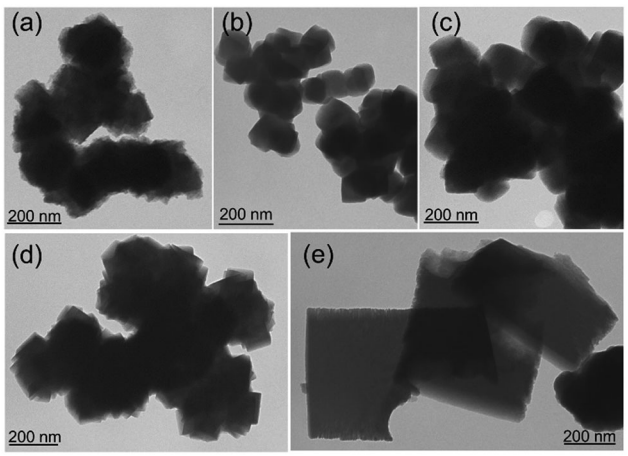

Fig. 2 TEM images of the samples with UiO-66 (1:2:0_120-UiO, 1:2:3_120-UiO, 1:1:3_120-UiO, and 1:2:3_220-UiO: parts (a)–(d), respectively) and MIL-140A (1:2:0_220-MIL) part (e) structures.

UiO-66,[11,29] while samples 1:2:0_220-MIL and 1:1:0_220-amor show the vibrational fingerprints of MIL-140A,[31] see the distinct vibrational envelope in the 600–500 cm^{-1} region. The FTIR data indicate that the absence of water at 220 °C leads to the formation of a material having the short-range order of MIL-140A, missing the long-range one that can be reached in the presence of an excess of linker. The materials characterization has been completed with TGA and N_2-adsoprtion studies (Fig S2 and S3, respectively in ESI†) obtaining results in line with the literature values for UiO-66 or MIL-140A.

Transmission electron microscopy (TEM) revealed that the synthesis conditions affect the crystal shape, as shown in Fig. 2. With the only exception of the 1:2:0_120-UiO sample, exhibiting crystals with ill-defined shapes (TEM projection which shows unstructured faces, see Fig. 2a), all other UiO-66 samples (Fig. 2b–d) consist of well-defined uniform square bipyramidal particles[32–35] visualized in the TEM projection as polyhedra with sharp faces of about 100–150 nm. These observations are in good agreement with XRPD analysis where the 1:2:0_120-UiO sample is distinguished by poorer crystallinity (Fig. 1a). Sample 1:2:0_220-MIL, resulting in the MIL-140A phase, appears as rectangular flat crystals of about 500–1000 nm (Fig. 2e).

Reviewing the products obtained in the 220 °C-syntheses, (Fig. 1c, d, 2d, e and Table 1), water appears as the key controlling factor in driving the products towards the UiO-66 or MIL-140A phases. To understand the role of water, two additional experiments were performed by adding ZrO_2 nanoparticles (NPs) in both monoclinic (M-ZrO_2) and tetragonal (T-ZrO_2) forms in the water-free synthesis batches: samples 1:2:0_220_M-ZrO_2-MIL and 1:2:0_220_T-ZrO_2-UiO, respectively (Table 1). Addition of a small amount of T-ZrO_2 results in the formation of UiO-66, while addition of M-ZrO_2 does not significantly affect the obtained product, as testified by the XRPD patterns reported in Fig. 3a. In the former case, almost complete absence of the (022) reflection indicates the formation of a UiO-66 phase having dehydroxylated distorted Zr_6O_6 octahedra

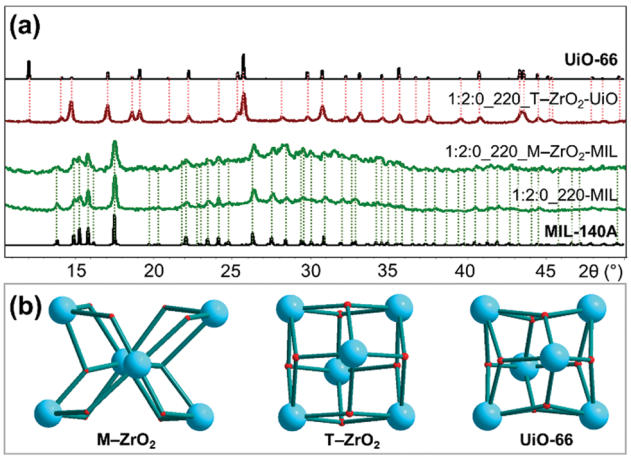

Fig. 3 Part (a): XRPD profiles (λ = 1.5406 Å) of samples synthesized at 220 °C with and without addition of ZrO_2 NPs. See Fig. S1c in ESI† for the full patterns including (111) and (002) reflections. Part (b): sticks and ball representation of zirconium-oxygen clusters (Zr blue and O red: the size of the O balls was minimized to highlight the position of Zr) in the monoclinic and tetragonal forms of ZrO_2 and in the UiO-66 SBU, from left to right.

as SBUs.[11,29,30] In the latter case, the reflections of M-ZrO_2 remain traceable in the XPRD profile (dominated by the MIL-140A peaks) of the final product, indicating that the additive has not been consumed during the reaction. No reflection of T-ZrO_2 was observed in the pattern of 1:2:0_220_T-ZrO_2-UiO sample, suggesting that the Zr atoms of T-ZrO_2 additive were included in the UiO-66 framework.

It is worth mentioning that the addition of metal oxide NPs in the reaction batch may modify the synthesis of UiO-MOFs as testified by Han *et al.*[36] who showed that the addition of Cu_2O NPs provided a way for tuning the crystal size.

By cutting a Zr_6O_8 cluster from the M-ZrO_2 and T-ZrO_2 crystals and comparing them with the UiO-66 SBU (Fig. 3b) it becomes evident that T-ZrO_2 NP exhibits a local arrangement of Zr and O atoms that is very close to that present in the UiO-66 SBU, while monoclinic phase does not. The obtained results (Fig. 3a and Table 1) can therefore be explained assuming that the BDC ligand can interact with the surface of T-ZrO_2 NPs. In this way, 1:2:0_220_T-ZrO_2-UiO will act as a nucleation starting seed for the UiO-66 phase, which prevails over the MIL-140A one. The addition of M-ZrO_2 NPs does not affect the nature of the products, which remain unaltered at the end of the synthesis. It is interesting to note that at the end of a TGA experiment on UiO-66, the remaining solid phase is a low crystalline form of ZrO_2 exhibiting a broad peak around $2\theta \approx 30^\circ$ (Cu Kα),[11,13,34] corresponding to the (011) reflection of the T-ZrO_2 phase (see Fig. S4 in ESI†). The thermal decomposition of UiO-66 into T-ZrO_2 can be somehow considered as the inverse reaction that leads to UiO-66 formation in synthesis 1:2:0_220_T-ZrO_2-UiO.

These observations are the key to understand the role of water in the standard syntheses of Zr-BDC MOFs. It is indeed known that water interacts with zirconium tetrachloride to form zirconia and hydrochloric acid:[37–41]

$$ZrCl_4 + 2H_2O \rightarrow ZrO_2 + 4HCl \quad (1)$$

Reaction (1) is exothermic with a ΔG of −144 kJ mol^{-1} at 300 °C.[38] Different forms of zirconia (cubic, monoclinic and tetragonal) were observed in the experiments reported in the literature,[37–41] depending on the growth temperature (T) and on the size (d) of the particles obtained at the end of the growth. In the (T,d) plane of the zirconia phase diagram, the monoclinic form is the most stable at low T and at large d regions, while the tetragonal form reveals at the beginning of the growth or where d remains small.[39,41,42]

Eqn (1) applies for the growth of a macroscopic ZrO_2 phase, as no competitive reactions can occur in the environment described in the quoted references,[37–41] besides the crystal size-driven tetragonal to monoclinic phase transition. In the case of the Zr-BDC MOFs synthesis the growth of the ZrO_2 phase is prevented by H_2BDC linkers that block the propagation of the oxide phase from the beginning. Keeping in mind that Cl^- has been reported to coordinate the UiO-66 SBU in some synthesis,[16] a plausible reaction path of UiO in presence of water is:

$$6ZrCl_4 + (18 - x)H_2O \rightarrow Zr_6O_6(OH)_{12-x}Cl_x + (24 - x)HCl \ (0 \le x \le 12) \quad (2)$$

where the precursor of the SBU of UiO-66 starts being formed with the dangling bonds of the Zr atoms saturated by OH^- and Cl^- ligands. This "proto"-SBU units can progressively react with the H_2BDC linkers to form the known $[Zr_6O_4(OH)_4]^{12+}$ SBU, with twelve $HBDC^-$ linkers coordinated to it:

$$Zr_6O_6(OH)_{12-x}Cl_x + 12H_2BDC \rightarrow Zr_6O_4(OH)_4(HBDC)_{12} + (10 - x)H_2O + xHCl \quad (3)$$

Each $HBDC^-$ linker in eqn (3) still possess the –COOH group at the opposite sides to coordinate a different SBU and propagate the growth of the UiO-66 crystal. A graphical representation of reactions (2) and (3) is reported in Fig. 4 with x = 6. Note that the formation of UiO-66 from methacrylate oxocluster $Zr_6O_4(OH)_4(OMc)_{12}$ (OMc=CH_2=$CH(CH_3)$COO) is known.[43]

On this basis, it is evident that addition of water to the Zr-BDC MOFs synthesis causes the formation of ZrO_2 NPs upon interaction with $ZrCl_4$ according to eqn (1)–(3). As formed, the ZrO_2 NPs are in the tetragonal form because of their small size, eqn (1). The possible successive transformation to the monoclinic form, by size increase, is prevented due to the presence of the BDC linkers, which will direct the growth into the UiO-66 phase, eqn (2) and (3), as in the synthesis of the 1:2:0_220_T-ZrO_2-UiO sample.

At 220 °C, where two different MOF structures can be obtained, the presence or the absence of T-ZrO_2 NPs (either directly inserted

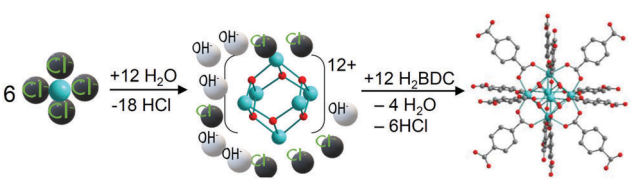

Fig. 4 Graphical representation of reactions (2) and (3) with x = 6.

in the reaction mixture or formed *in situ via* eqn (1)) will drive the products towards the UiO-66 or the MIL-140A phases, respectively. At 120 °C, where MIL-140A cannot be formed, even in absence of intentionally added water, minor moisture contamination, or a different growth mechanism, will result into a slow growth of the UiO-66 phase with ill-defined crystallinity. Recently, the amount of added water and the aging of the reaction mixture was exploited to tune the UiO-66 crystal size in the 10–125 nm size.[44]

Summarizing, we highlighted the role of water in the nucleation processes of the Zr-BDC MOFs system: H_2O interacts with $ZrCl_4$ with the formation of T-ZrO_2 NPs,[37–41] eqn (1), that act as seeds for the UiO-66 growth, as they exhibit Zr_6O_8 clusters with a local arrangement of Zr and O atoms very close to that of the UiO-66 SBU (Fig. 3b). This thesis has been proven by performing *ad hoc* experiments where M-ZrO_2 and T-ZrO_2 NPs were intentionally added to the water-free reaction mixture.

This study was supported by the grant 16.3871.2017/4.6 of the Ministry of Education and Science of the Russian Federation.

Conflicts of interest

There are no conflicts to declare.

Notes and references

1 A. U. Czaja, N. Trukhan and U. Muller, *Chem. Soc. Rev.*, 2009, **38**, 1284.
2 J. R. Li, R. J. Kuppler and H. C. Zhou, *Chem. Soc. Rev.*, 2009, **38**, 1477.
3 A. Corma, H. Garcia and F. Xamena, *Chem. Rev.*, 2010, **110**, 4606.
4 *Metal-Organic Frameworks: Applications from Catalysis to Gas Storage*, ed. D. Farrusseng, Wiley, Weinheim, 2011.
5 H. Furukawa, K. E. Cordova, M. O'Keeffe and O. M. Yaghi, *Science*, 2013, **341**, 974.
6 F. X. Llabres i Xamena and J. Gascon, *Metal Organic Frameworks as Heterogeneous Catalysts*, Royal Society of Chemistry, Cambridge, 2013.
7 V. V. Butova, M. A. Soldatov, A. A. Guda, K. A. Lomachenko and C. Lamberti, *Russ. Chem. Rev.*, 2016, **85**, 280.
8 O. M. Yaghi, M. O'Keeffe, N. W. Ockwig, H. K. Chae, M. Eddaoudi and J. Kim, *Nature*, 2003, **423**, 705.
9 T. A. Makal, A. A. Yakovenko and H. C. Zhou, *J. Phys. Chem. Lett.*, 2011, **2**, 1682.
10 J. H. Cavka, S. Jakobsen, U. Olsbye, N. Guillou, C. Lamberti, S. Bordiga and K. P. Lillerud, *J. Am. Chem. Soc.*, 2008, **130**, 13850.
11 L. Valenzano, B. Civalleri, S. Chavan, S. Bordiga, M. H. Nilsen, S. Jakobsen, K. P. Lillerud and C. Lamberti, *Chem. Mater.*, 2011, **23**, 1700.
12 S. Oien, D. Wragg, H. Reinsch, S. Svelle, S. Bordiga, C. Lamberti and K. P. Lillerud, *Cryst. Growth Des.*, 2014, **14**, 5370.
13 G. C. Shearer, S. Chavan, J. Ethiraj, J. G. Vitillo, S. Svelle, U. Olsbye, C. Lamberti, S. Bordiga and K. P. Lillerud, *Chem. Mater.*, 2014, **26**, 4068.
14 G. C. Shearer, S. Chavan, S. Bordiga, S. Svelle, U. Olsbye and K. P. Lillerud, *Chem. Mater.*, 2016, **28**, 3749.
15 K. B. Lausund and O. Nilsen, *Nat. Commun.*, 2016, **7**, 13578.
16 M. G. Goesten, M. F. de Lange, A. I. Olivos-Suarez, A. V. Bavykina, P. Serra-Crespo, C. Krywka, F. M. Bickelhaupt, F. Kapteijn and J. Gascon, *Nat. Commun.*, 2016, **7**, 11832.
17 C. Atzori, G. C. Shearer, L. Maschio, B. Civalleri, F. Bonino, C. Lamberti, S. Svelle, K. P. Lillerud and S. Bordiga, *J. Phys. Chem. C*, 2017, **121**, 9312.
18 V. Guillerm, F. Ragon, M. Dan-Hardi, T. Devic, M. Vishnuvarthan, B. Campo, A. Vimont, G. Clet, Q. Yang, G. Maurin, G. Ferey, A. Vittadini, S. Gross and C. Serre, *Angew. Chem., Int. Ed.*, 2012, **51**, 9267.
19 W. B. Liang, R. Babarao and D. M. D'Alessandro, *Inorg. Chem.*, 2013, **52**, 12878.
20 M. Kandiah, S. Usseglio, S. Svelle, U. Olsbye, K. P. Lillerud and M. Tilset, *J. Mater. Chem.*, 2010, **20**, 9848.
21 S. Chavan, J. G. Vitillo, M. J. Uddin, F. Bonino, C. Lamberti, E. Groppo, K. P. Lillerud and S. Bordiga, *Chem. Mater.*, 2010, **22**, 4602.
22 S. Øien, G. Agostini, S. Svelle, E. Borfecchia, K. A. Lomachenko, L. Mino, E. Gallo, S. Bordiga, U. Olsbye, K. P. Lillerud and C. Lamberti, *Chem. Mater.*, 2015, **27**, 1042.
23 L. Braglia, E. Borfecchia, K. A. Lomachenko, A. L. Bugaev, A. A. Guda, A. V. Soldatov, B. T. L. Bleken, S. Oien, U. Olsbye, K. P. Lillerud, S. Bordiga, G. Agostini, M. Manzoli and C. Lamberti, *Faraday Discuss.*, 2017, **201**, 265.
24 E. S. Gutterod, S. Oien-Odegaard, K. Bossers, A. E. Nieuwelink, M. Manzoli, L. Braglia, A. Lazzarini, E. Borfecchia, S. Ahmadigoltapeh, B. Bouchevreau, B. T. Lonstad-Bleken, R. Henry, C. Lamberti, S. Bordiga, B. M. Weckhuysen, K. P. Lillerud and U. Olsbye, *Ind. Eng. Chem. Res.*, 2017, **56**, 13207.
25 A. L. Bugaev, A. A. Guda, K. A. Lomachenko, E. G. Kamyshova, M. A. Soldatov, G. Kaur, S. Øien-Ødegaard, L. Braglia, A. Lazzarini, M. Manzoli, S. Bordiga, U. Olsbye, K. P. Lillerud, A. V. Soldatov and C. Lamberti, *Faraday Discuss.*, 2018, **208**, 287.
26 S. Smolders, K. A. Lomachenko, B. Bueken, A. Struyf, A. L. Bugaev, C. Atzori, N. Stock, C. Lamberti, M. B. J. Roeffaers and D. E. De Vos, *ChemPhysChem*, 2018, **19**, 373.
27 S. Waitschat, D. Frohlich, H. Reinsch, H. Terraschke, K. A. Lomachenko, C. Lamberti, H. Kummer, T. Helling, M. Baumgartner, S. Henningerb and N. Stock, *Dalton Trans.*, 2018, **47**, 1062.
28 K. A. Lomachenko, J. Jacobsen, A. L. Bugaev, C. Atzori, F. Bonino, S. Bordiga, N. Stock and C. Lamberti, *J. Am. Chem. Soc.*, 2019, **141**, DOI: 10.1021/jacs.8b10343.
29 S. Chavan, J. G. Vitillo, D. Gianolio, O. Zavorotynska, B. Civalleri, S. Jakobsen, M. H. Nilsen, L. Valenzano, C. Lamberti, K. P. Lillerud and S. Bordiga, *Phys. Chem. Chem. Phys.*, 2012, **14**, 1614.
30 S. Jakobsen, D. Gianolio, D. S. Wragg, M. H. Nilsen, H. Emerich, S. Bordiga, C. Lamberti, U. Olsbye, M. Tilset and K. P. Lillerud, *Phys. Rev. B: Condens. Matter Mater. Phys.*, 2012, **86**, 125429.
31 B. Van de Voorde, I. Stassen, B. Bueken, F. Vermoortele, D. De Vos, R. Ameloot, J. C. Tan and T. D. Bennett, *J. Mater. Chem. A*, 2015, **3**, 1737.
32 Q. Zhao, W. Yuan, J. M. Liang and J. P. Li, *Int. J. Hydrogen Energy*, 2013, **38**, 13104.
33 Y. R. Miao, Z. Su and K. S. Suslick, *J. Am. Chem. Soc.*, 2017, **139**, 4667.
34 V. V. Butova, A. P. Budnyk, A. A. Guda, K. A. Lomachenko, A. L. Bugaev, A. V. Soldatov, S. M. Chavan, S. Oien-Odegaard, U. Olsbye, K. P. Lillerud, C. Atzori, S. Bordiga and C. Lamberti, *Cryst. Growth Des.*, 2017, **17**, 5422.
35 D. F. S. Gallis, J. A. Harvey, C. J. Pearce, M. G. Hall, J. B. DeCoste, M. K. Kinnan and J. A. Greathouse, *J. Mater. Chem. A*, 2018, **6**, 3038.
36 Y. T. Han, M. Liu, K. Y. Li, Q. Sun, C. S. Song, G. L. Zhang, Z. C. Zhang and X. W. Guo, *Cryst. Growth Des.*, 2017, **17**, 685.
37 J. Aarik, A. Aidla, H. Mandar, T. Uustare and V. Sammelselg, *Thin Solid Films*, 2002, **408**, 97.
38 A. Rahtu and M. Ritala, *J. Mater. Chem.*, 2002, **12**, 1484.
39 J. C. Valmalette and M. Isa, *Chem. Mater.*, 2002, **14**, 5098.
40 R. Septawendar, B. S. Purwasasmita, S. Sutardi, N. Sofyaningsih and W. Kristanto, *J. Ceram. Process. Res.*, 2012, **13**, 343.
41 V. Miikkulainen, M. Leskela, M. Ritala and R. L. Puurunen, *J. Appl. Phys.*, 2013, **113**, 101.
42 P. Bouvier, E. Djurado, C. Ritter, A. J. Dianoux and G. Lucazeau, *Int. J. Inorg. Mater.*, 2001, **3**, 647.
43 V. Guillerm, S. Gross, C. Serre, T. Devic, M. Bauer and G. Ferey, *Chem. Commun.*, 2010, **46**, 767.
44 M. Taddei, K. C. Dumbgen, J. A. van Bokhoven and M. Ranocchiari, *Chem. Commun.*, 2016, **52**, 6411.

